Instituto Tecnológico y de Estudios Superiores de Monterrey

Campus Monterrey

School of Engineering and Sciences

Effects of atmospheric stability conditions on the pollutants dispersion near roads using CFD

A thesis presented by

David Sebastián Martínez Toxtle

Submitted to the
School of Engineering and Sciences
in partial fulfillment of the requirements for the degree of

Master of Science

In

Engineering Science

Monterrey Nuevo León, December 10th, 2019

Instituto Tecnológico y de Estudios Superiores de Monterrey

Campus Monterrey

School of Engineering and Sciences

The committee members, hereby, certify that have read the thesis presented by David Sebastián Martínez Toxtle and that it is fully adequate in scope and quality as a partial requirement for the degree of Master of Science in Engineering Science

Dr. José Ignacio Huertas Cardozo
Tecnológico de Monterrey
School of Engineering and Sciences
Principal Advisor

Dr. José Luis López Salinas
Tecnológico de Monterrey
School of Engineering and Sciences
Committee Member

Tecnológico de Monterrey
10 DIC 2019
Dirección Nacional de Posgrado
Dr. Rubén Morales Menéndez

Dr. Gabriel Cuevas Figueroa
Tecnológico de Monterrey
School of Engineering and Sciences
Committee Member

Dr. Rubén Morales Menéndez
Dean of Graduate Studies
School of Engineering and Sciences

Monterrey Nuevo León, December 10th, 2019

Declaration of Authorship

I, David Sebastián Martínez Toxtle, declare that this thesis titled, Effects of atmospheric stability conditions on the pollutants dispersion near roads using CFD and the work presented in it are my own. I confirm that:

- This work was done wholly or mainly while in candidature for a research degree at this University.
- Where any part of this thesis has previously been submitted for a degree or any other qualification at this University or any other institution, this has been clearly stated.
- Where I have consulted the published work of others, this is always clearly attributed.
- Where I have quoted from the work of others, the source is always given. With the exception of such quotations, this thesis is entirely my own work.
- I have acknowledged all main sources of help.
- Where the thesis is based on work done by myself jointly with others, I have made clear exactly what was done by others and what I have contributed myself.

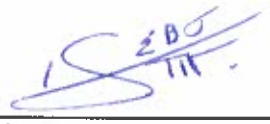

David Sebastián Martínez Toxtle
Monterrey Nuevo León, December 10th, 2019

Dedication

To my family and all those who have supported me through this process

Acknowledgements

This work was possible thanks to the resources, infrastructure and support provided by Tecnologico de Monterrey, Energy and Climate Change Research group and CONACyT.

I would like to express my sincere gratitude to my advisor Dr. José Ignacio for the continuous support during my studies and research, for his patience, motivation, enthusiasm, and immense knowledge. His guidance helped me in all the time of research and in times of need.

I gratefully acknowledge the contributions to my thesis from the committee, Dr José Luis López and Dr. Gabriel Cuevas

To all my fellow colleagues at the Energy and Climate Change Research group and the master's in engineering science program for their support in my personal and professional growth.

And last but not least to God for the gift of life and this second chance to living it, to my family for the encouragement and support through this process.

Effects of atmospheric stability conditions on the pollutants dispersion near roads using CFD

by

David Sebastián Martínez Toxtle

Abstract

This study quantifies the effects of atmospheric stability conditions on the concentration of atmospheric pollutants near roads. We used as a base case scenario the resulting concentrations obtained solving numerically the physics equations that describe the dispersion of pollutants emitted from a road located on a flat terrain under neutral atmospheric conditions i.e. uniform temperature and isotropic turbulence. Then, we added to this model the Monin-Obukhov similarity theory (MOST), which describes the complex interactions between solar radiation, earth surface, and local air flows under different atmospheric stability conditions and fixes the resulting profiles for wind velocity, ambient temperature, and turbulence. We found that the near road concentrations of gas and solid phase pollutants under different stability conditions are highly correlated (R^2>0.91) to the concentrations observed downwind the road under neutral conditions. However, when the atmosphere is highly stable or stable, these concentrations are 30% and 7%, respectively, higher than the observed under neutral conditions. Similarly, when the atmosphere is extremely unstable or unstable, the concentrations values are 8% and 7%, respectively, lower than the observed under neutral conditions. Our results are of great relevance for the design of living or artificial barriers located on the sides of the road as an adaptive countermeasure to protect the health of pedestrians or residents living near roads.

Keywords: Pollutant dispersion, Air quality modeling, Computational Fluid Dynamics.

List of Figures

List of Tables

Contents

Chapter 1

Introduction

1.1 Motivation

In urban centers, the vehicles are the main source of fine (d <10 μm) and ultrafine (d <100 nm) particles, black carbon, carbon monoxide (CO), and nitrogen oxides (NOx) (Karner et al, 2010; EU,2015; Singh et al, 2018). Those air pollutants cause respiratory and cardiovascular problems, chronic diseases and early mortality on the people exposed to theses pollutants (McConnell et al., 2006; Niita et al., 1993; Pearson, Wachtel, & Ebi, 2000; Riediker et al., 2004). Studies have shown that within the urban regions, pedestrians and people living near roads (< 500 m) are exposed to the highest concentration levels of these pollutants (Finn et al, 2009). Therefore, there is an urgent need for the design of countermeasures to reduce pollutant concentration near roads. For example, it has been found that the use of natural or human made barriers located on the sides of the roads has the potential of reducing those concentrations near roads (Baldauf et al., 2016; Hagler et al., 2012; Ranasinghe et al., 2017; Tong et al., 2016). However, the improper design of those barriers could end up increasing those concentrations or moving the concentration peaks to some distance downwind the road.

1.2 Problem Statement and Context

It has been reported that atmospheric stability conditions play an important role in the pollutants dispersion, nevertheless this effects have not been systematically quantified because of the complexity in the data acquisition due to the nature of the atmosphere, in which is possible no to have the same atmospheric condition in consecutive days.

CFD-based models can be used to evaluate systematically the effects of different atmospheric stability conditions on the dispersion of pollutants. Few works have been conducted with this objective in mind. Using CFD, Pieterse et al (2013) evaluated the effects of three atmospheric stability conditions on the homogeneous horizontal flow over a flat terrain. They found the parameters for the *k-e* turbulence model that describes those atmospheric conditions. However, they did not study the effects of atmospheric stability on the dispersion of pollutants. Steffens et al. (2012) replicated the experimental work conducted by Finn et al (2009) studying the effect of the atmospheric stability conditions on the dispersion of HS_6 across a barrier. They modelled the atmospheric stability conditions by implementing the Monin Obukhov Similarity Theory (MOST) and evaluated the performance of two turbulence models: Reynolds Average Navier Stokes (RANS) and Large Eddie Simulation (LES). They found that both models produced similar results. They did not quantify the effect of the atmospheric stability conditions on the dispersion of the trace gas.

The effects of the atmospheric stability condition on pollutant dispersion can also be studied experimentally. Few studies have been conducted aiming to quantify those effects. Zoras et al. (2006) used 2 years period of meteorological and PM_{10} concentration data in a region (50 km^2) in Greece where a coal plant was a main source of pollutants. They observed that most of the PM_{10} episodes (42.6%) occurred when the atmosphere was extremely stable (F). Aiming to quantify the effects of roadside barriers on the downwind dispersion of atmospheric pollutants emitted by roadway sources, in 2008, the National Oceanic Atmospheric Administration (NOOA) at the Idaho National Laboratory (USA) dispersed SF_6 and measured the concentration of this trace gas at several positions downwind a solid barrier. They observed that the SF_6 concentrations downwind, with and without barrier were higher when the atmosphere was stable compare with when it was neutral or unstable (Finn et al. 2010). In the same year (2008), the Environmental Monitoring Center of Lanzhou (China), monitored for 11 months meteorological and pollutant concentrations at three contrasting sites and used the radon-based technique to monitor atmospheric stability. They assumed that emissions in the city remained constant thorough the year and compared the morning air pollutant concentrations to isolate the effects of the diurnal changes in the mean mixing depth. They found that the morning peaks of pollutants concentrations increased by a factor of 2-5 from the most well-mixed to stable atmospheric conditions (Wang et al., 2016). All these experimental works agree that pollutant concentration is higher under stable atmospheric conditions that under unstable condition. However, the magnitude of this effect varies among experimenters. Furthermore, the experimental measurements can not be used to quantify the effects of the atmospheric stability isolated from variations in meteorological conditions and therefore they cannot be used for modelling purposes.

1.3 Research Question

The current models used in regulatory processes for air quality in the microscale (RLINE, AERMOD) present accurate results over long periods of time (> 1 year) and in neutral atmospheric conditions.

The development of a reliable model requires the study and understanding of atmospheric dynamics, as well as the processes of transport and sedimentation of pollutants. Recently different models have been coupled to make a better representation of the atmosphere however this has not been fully developed in a CFD software

CFD allows us to develop a model that is able to systematically quantify the effects of atmospheric stability on the dispersion of pollutants. In this study, we intend to answer the following questions.

• Is it possible to reproduce atmospheric dynamics in a reduced computational domain?

• How can the effects of atmospheric stability on the pollutant dispersion be systematically assessed?

• What are the effects of the atmospheric stability conditions on the pollutant concentration in the downwind direction?

1.4 Solution overview

To address these research questions, it is proposed to perform a series of simulations in a commercial CFD software to represent the different atmospheric stability conditions based in the Monin-Obukhov Similarity Theory in a reduced computational domain to evaluate the effects of atmospheric stability conditions on TSP dispersion. Subsequently, this effect will be determined based on different performance evaluation models such as Fractional Bias (FB), Geometric Bias (GB) and error-based models such as Root Mean Square Error (RMSE), Normalized Mean Square Error (NMSE).

1.5 Structure of the Thesis

This work will be divided into two main sections in which the concepts of stability conditions and atmospheric stability conditions will be described, in section 3 the methodology used for CFD computational simulations and their evaluation will be presented and finally the conclusions section will be presented highlighting the contributions of this work.

Chapter 2 presents the concepts of atmospheric stability conditions, atmospheric dynamics and the fundamental equations that describe the process of emission, transport and deposition of pollutants.

Chapter 3 details the methodology used for the simulation of the stability conditions in a reduced computational domain in a commercial CFD software, as well as for the evaluation carried out to know the differences between the stability conditions.

Chapter 2

Dispersion process

2.1 Atmospheric Boundary Layer

The troposphere extends from the ground up to an average altitude of 11 km, but often only the lowest 2-3 kilometers are directly modified by the underlying surface. The atmospheric boundary layer is defined as that part of the troposphere that is directly influenced by the presence of the earth's surface and responds to surface forcings such as heat transfer and evaporation. (Stull,2005). Is in this layer where the dispersion of pollutants phenomena occurs (emission, transport, reaction and deposition). The atmospheric boundary layer thickness is variable in time and space ranging from 100m to 3km.
The last meters (~10%) of the atmospheric boundary layer is called the Surface Layer (SL), this sublayer is highly influenced for both wind flow turbulence and buoyant turbulence. This study is focused in reproducing the atmospheric dynamics inside this sublayer.

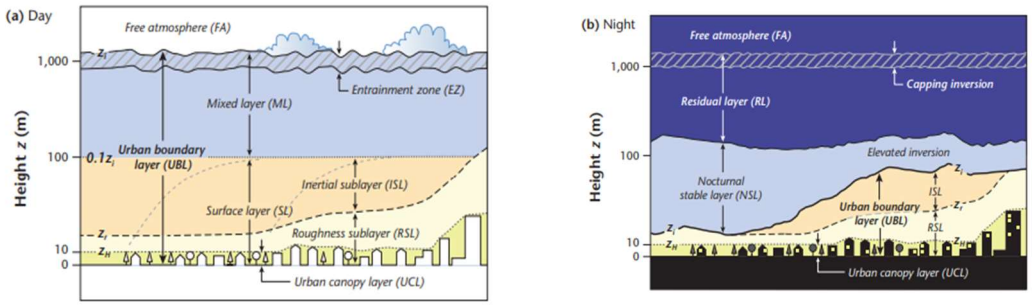

Figure 2. 1 Evolution of the ABL through a day taken from (Oke, 1988).

The influence of this surface forcings are transmitted to the ABL by the mechanism of turbulence. Mass, momentum and energy are also transmitted to the ABL by turbulence.

2.2 Atmospheric stability conditions

Atmospheric stability refers to the ability of the atmosphere to be turbulent, which you can determine from soundings of temperature, humidity, and wind. Turbulence and stability vary with time and place because of the corresponding variation of the soundings. (Stull, 2018)

Atmospheric stability plays the most important role in the transport and dispersion of pollutants. Generally, the difficulty involved in measuring atmospheric stability causes it to not to be evaluated. However, different methods are used for stability determination with varying degrees of complexity (Mohan and Siddiqui, 1998; Zoras et al., 2006)

2.2.1 Static Stability

The dominant process in the lower atmosphere is convection. A major control on the type and extent of convective activity is the vertical temperature structure. Static stability controls formation of the ABL and affects ABL wind and temperature profiles. (Stull, 2005). The

variation of temperature with altitude in the atmosphere is an important parameter to determine the degree to which material will mix vertically. (Seinfeld and Pandis, 2006)

Consider a discrete parcel of air moving up through the atmosphere and assume that it neither receives nor gives out heat to the surrounding air (adiabatic). As it rises it encounters lower atmospheric pressure because the mass of air above it becomes progressively less. Thus, the internal pressure of the parcel becomes greater relative to its surroundings and the parcel will tend to expand. To push away the surrounding air requires work and therefore energy. But the only energy available is the thermal energy of the parcel itself, thus as the parcel rises it cools down. In dry (unsaturated) air the rate of temperature change of such a parcel with height is the constant value of $9{\cdot}8\times10^{-3}$ °C m^{-1} called the dry adiabatic lapse rate (Γ)(1). (Oke, 1988)

The lapse rate in the lower portion of the atmosphere has a great influence on the vertical motion of air. Buoyancy can resist or enhance vertical air motion of airmasses, affecting the mixing of pollutants. (Seinfeld and Pandis, 2006)

Comparing the environmental lapse rate (Λ) (2), which is the local temperature lapse rate in a determined location normally measured with meteorological towers, with the adiabatic lapse rate, three regimes of atmospheric stability can be defined shown in table 2.2.1.

$$\Gamma = -\left(\partial T/\partial z\right)_{adiabatic} = -\rho/c_p \qquad (1)$$

$$\Lambda = \partial T/\partial z \qquad (2)$$

Table 2.2.1 Static atmospheric stability conditions (Arya,1988)

Lapse rate	Atmospheric stability
$\Lambda < \Gamma$:	Unstable
$\Lambda = \Gamma$:	Neutral
$\Lambda > \Gamma$:	Stable

a. b.

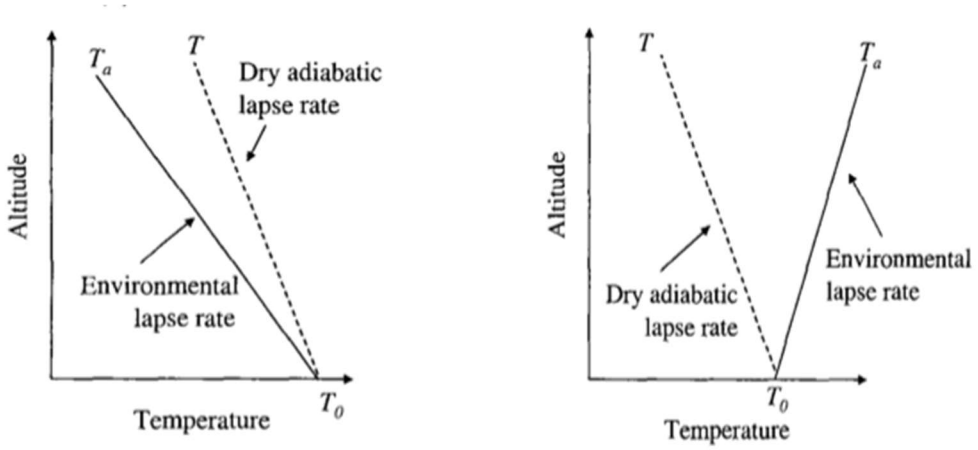

Figure 2. 2 Temperature profiles for a) atmosphere statically unstable and b) atmosphere statically stable taken from (Seinfeld and Pandis, 2006)

Nevertheless, even if the air is statically stable, wind shears may be able to generate turbulence dynamically, thus, the measurement of the temperature gradient is not enough to determine the local atmospheric stability.

2.2.2 Dynamic stability

Dynamic stability considers both buoyancy and wind shear to determine whether the flow will become turbulent. Wind shear is the change of wind speed or direction with height and can be squared to indicate the kinetic energy available to cause turbulence. (Sutll, 2015)

Different methods are used for stability determination with varying degrees of complexity, most of them compares the buoyant induced turbulence to mechanical induced turbulence ratio.

Generally, when the buoyant induced turbulence is predominant, wind speed is low, and the atmosphere is in an unstable condition. When mechanical turbulence increases, and the buoyant produced turbulences is less than mechanical turbulence the atmosphere tends to a neutral condition. Finally, in absence of buoyant produced turbulence, mechanical turbulence is absorbed as result there is no vertical mixing, resulting in a stable atmospheric condition.

In this study, some dynamic stability classification methods are presented, however, the presented model is focused in the MOST scheme.

2.2.2.1 Monin-Obukhov Similarity Theory

The similarity prediction that follows from the Monin–Obukhov similarity hypothesis is that any mean flow or turbulence quantity in the surface layer, when normalized by an appropriate scaling parameter, must be a unique function of z/L only (Arya, 2011).

Where L is the Obukhov's length that expresses the relative roles of shear and buoyancy in the production or consumption of turbulence kinetic energy, defined in (3)

$$L = -u_*^3/[k(g/T_0)(H_0/\rho c_p)] \quad (3)$$

Where $u_*$is the friction velocity, k is the Von Karman constant, usually with the value of 0.41, g represents the gravity, T_0 is the air temperature, H_0 is the heat flux from the surface (positive during the day and negative at night) C_p is the specific heat of air at constant pressure.

Wind speed: In the surface layer wind speeds increase roughly logarithmically (4) with height. Fiction generates that the mean windspeed close to the surface might be equal to zero. (Stull,2011)

$$u(z) = \left(\frac{u_*}{\kappa}\right)\left[ln\left(\frac{z}{z_0}\right) - \psi_m\left(\frac{z}{L}\right)\right] \quad (4)$$

Temperature: Temperature profiles in the SL also can be estimated following the similarity theory resulting in a vertical logarithmic profile described in (5) (De Visscher, 2014).

$$\theta(z) - \theta_0 = \left(\frac{\theta_*}{\kappa}\right)\left[ln\left(\frac{z}{z_0}\right) - \psi_h\left(\frac{z}{L}\right)\right] \quad (5)$$

Where $\theta_*$is the potential temperature, most of the time equal to T_0, z_0 is the roughness parameter, ψ_m and ψ_h are the are the integrated forms of the similarity functions, derived by (Businger et al. 1971; Dyer, 1974) and are given by (6) (7) (8)

$$\psi_m = \psi_h = -5\frac{z}{L} \qquad \text{for } \zeta \geq 0 \quad (6)$$

$$\psi_m = ln\left[\left(\frac{1+x^2}{2}\right)\left(\frac{1+x}{2}\right)^2\right] - 2\,tan^{-1}x + \frac{\pi}{2} \qquad \text{for } \zeta < 0 \quad (7)$$

$$\psi_h = 2ln\left(\frac{1+x^2}{2}\right) \qquad \text{for } \zeta < 0 \quad (8)$$

where $x = (1 - 15z/L)^{1/4}$

Under stable conditions the profiles are log linear and tend to become linear for large values of ζ. Under unstable conditions, ψ_m and $\psi_h$are positive, so that the deviations from the log law are of opposite sign. Consequently, the velocity and temperature profiles in the surface layer are expected to become more and more curvilinear as instability increases. (Arya, 1988)

Given the complexity to measure some parameters such as heat flow from the surface or the friction speed, some schemes were developed that facilitate the classification of atmospheric stability conditions such as the Pasquill scheme.

2.2.2.2 Pasquill-Gifford scheme

Recognizing the need for a readily usable way to define atmospheric stability based on routine observations, Pasquill (1961) proposed a discrete atmospheric stability classification scheme that was later modified by Turner (1969). The scheme relies on observations of near-surface (10m) wind, solar radiation, and cloudiness.

There are mainly six atmospheric stabilities designated as A (extremely unstable), B (unstable), C (slightly unstable), D (neutral), E (slightly stable), and F (extremely stable). Later, stability G is also included to represent low wind nighttime stable conditions (Mohan and Siddiqui,1998)

Table 2.2.2 Pasquill-Gifford Scheme (Turner, 1969)

Wind speed m/s (10 m height)	Day			Night	
	Incoming Solar radiation			Cloudiness	
	Strong	Moderate	Slight	≥ 4/8	≤ 3/8
< 2	A	A-B	B	-----	-----
2-3	A-B	B	C	E	F
3-5	B	B-C	C	D	E
5-6	C	C-D	D	D	D
>6	C	D	D	D	D

Incoming solar radiation: Strong (>700 Wm^{-2}), moderate (350-700 Wm^{-2}), slight (< 350 Wm^{-2})

Golder (1972) established a relation among the Pasquill stability classes, the roughness length z_o. With the relation shown in (9) and the parameters for the coefficients a and b shown in Table 2.2.3 Obukhov's length can be determined from Pasquill's scheme

$$1/L = a + b \log z_0 \qquad (9)$$

Table 2.2 3 Correlation parameters to estimate Obukhov's length (Seinfeld and Pandis, 2005)

	Coefficients	
Stability Condition	a	b
A (Extremely unstable)	- 0.096	0.029
B (Unstable)	- 0.037	0.029
C (Slightly unstable)	- 0.002	0.018
D (Neutral)	0	0
E (Slightly stable)	0.004	- 0.018
F (Extremely stable)	0.035	- 0.036

Table 2.2.4 presents the relation between Monin Obukhov stability scheme and Pasquill-Gifford stability scheme. The advantages of Pasquill's stability classification scheme are its simplicity and reliance on measurements that are available. As a result, it is the most frequently used scheme for characterization of atmospheric turbulence. Its most important limitation is its discrete nature, covering a wide range of atmospheric conditions with only six classes. As a result, a wide range of conditions is covered by each class, resulting in a range of potential values of L and other parameters that can be calculated for given atmospheric conditions. (Seinfeld and Pandis, 2006)

Table 2.2.4 Monin Obukhov's and Pasquill-Gifford's Stability conditions schemes (Seinfeld and Pandis, 2006; Ashrafi and Hoshyaripour)

Stability Condition	Monin-Obukhov	Pasquill-Gifford
Extremely unstable	$-100 < L < 0$	A
Unstable		B
Slightly unstable	$-10^5 < L < -100$	C
Neutral	$\|L\| > 10^5$	D
Slightly Stable	$10 < L < 10^5$	E
Extremely Stable	$0 < L < 10$	F

2.3 Atmospheric turbulence

Turbulence is important because it mixes and churns the atmosphere and causes water vapor, smoke, and other substances, as well as energy, to become distributed both vertically and horizontally.

By nature, the wind flow is turbulent, it is irregular and varies randomly over time. Some general characteristics of turbulence are irregularity or randomness, three-dimensional and highly rotating, diffusive, dissipative and multiplicity.

This randomness can be considered as the generation and disappearance of eddies (rotating air masses) that transfer momentum, heat, and mass between adjacent air parcels. (De Visscher, 2013)

These eddies are caused by many different phenomena:

- Convection: If the lower parts of the atmosphere heat up, the atmosphere can become convectively unstable, leading to convective bubbles of gas rising to higher altitudes. Often these bubbles produce cumulus clouds, the strongest of which, the cumulonimbus clouds, cause lightning storms. But not all convection leads to clouds, and convection happens on all scales. For instance, if an asphalt road gets heated up by intense sunlight, the few centimeter-thick layers of air above it convectively rise, while cooler air sinks.

- Wind shear: is the difference in wind speed or direction over a relatively short distance in the atmosphere, is most often associated with strong temperature inversions or density gradients. Wind shear can occur at high or low altitude.

    - Wind shear from temperature inversions: Overnight cooling creates a temperature inversion a few hundred meters above the ground. This inversion can produce significant wind shear close to the ground.

    - Wind shear from surface obstructions: When the air near the surface of the Earth flows over obstructions, such as mountains, hills, trees, or buildings, the normal horizontal wind flow is disturbed and transformed into a complicated pattern of eddies and other irregular air movements. In urban context street canyons are the main source of mechanical induced turbulence.

2.4 Fundamental equations

Flows in the SL can be represented by the fundamental equations of fluid mechanics adjusted to the scale of the lower part of the atmosphere (Stull, 1988).

Derived equations that govern the fluid density, temperature and velocities in the SL are known as the fundamental equations for i) the mass-conservation or continuity equation (10),

ii) the momentum conservation equation (11), iii) the energy conservation equation (12). When modelling the SL, it is possible to use the Boussinesq approximation that express the equilibrium profiles of pressure, density and temperature as a function of the same parameter. Then, for incompressible fluids the following equations are obtained:

Continuity equation

$$\frac{\partial \rho}{\partial t} + \nabla \cdot (\rho\, \vec{v}) = 0 \qquad (10)$$

Where ρ is air density y $\vec{v}$ is the velocity vector with components in the three directions (u, v, w)

Momentum equation

The Navier-Stokes momentum equation that describes the flow in the SL is represented in (11), where Coriolis force is neglected and assuming that atmospheric air is an incompressible Newtonian fluid.

$$\frac{\partial (\rho \vec{v})}{\partial t} + \rho(\vec{v} \cdot \nabla)\vec{v} = -\nabla p + \nabla \cdot \tau + \rho \vec{g} \qquad (11)$$

Where ρ is air density, p is pressure, τ is the Reynolds stress tensor y $\vec{g}$ is the gravity term. The terms in que equations represents 1: storage of momentum 2: advection of momentum 3: pressure-gradient forces 4: influence of viscous stress and the last term accounts for the acceleration due to gravity forces (buoyancy)

Energy equation

The First Law of Thermodynamics describes the conservation of enthalpy, which includes contributions from both sensible and latent heat transport. In other words, the water vapor in air not only transports sensible heat associated with its temperature, but it has the potential to release or absorb additional latent heat during any phase changes that might occur. (Stull, 2005)

$$\frac{\partial \rho E}{\partial t} + \nabla \cdot (\rho \vec{v} E) = \nabla \cdot (k \nabla T) + \rho q - \nabla \cdot (\rho \vec{v}) + \vec{v}(\nabla \cdot \tau) + \nabla \vec{v} : \tau + \rho g \cdot \vec{v} \qquad (12)$$

Where 1: represents energy storage, 2: energy advection, 3: heat transfer by conduction, 4: heat generation, 5: work done by flow 6: work done by viscous flow 7: dissipation and 8: gravitational terms.

These equations represent the flow in the atmosphere and can be solved when selecting the proper turbulence model and boundary conditions for temperature, pressure and velocity.

3.2 Turbulence Settings

The minimum requirement of the turbulence model for thermally influenced ABL flows is that it should account for both shear and buoyancy produced turbulence (Pieterse and Harms, 2013). The k-ε turbulence model meets these requirements and has been widely used in ABL-related studies, so there are a lot of properties for k (turbulent kinetic energy) and ε (turbulent energy dissipation) for meteorological data (Alinot and Masson, 2005). For this study, the k-ε Std model incorporated in the Ansys Fluent. 17.2 with modifications was selected for this study.

The k-ε model adds two equations for k and ε in order to ensure the closure of the system, which are presented in (13) and (14) respectively

$$\frac{\partial}{\partial t}(\rho k) + \frac{\partial}{\partial x_i}(\rho k u_i) = \frac{\partial}{\partial x_j}\left[\left(\mu + \frac{\mu_t}{\sigma_k}\right)\frac{\partial k}{\partial x_j}\right] + G_k + G_b + \rho\varepsilon - Y_M + S_k \qquad (13)$$

$$\frac{\partial}{\partial t}(\rho \varepsilon) + \frac{\partial}{\partial x_i}(\rho \varepsilon u_i) = \frac{\partial}{\partial x_j}\left[\left(\mu + \frac{\mu_t}{\sigma_\varepsilon}\right)\frac{\partial \varepsilon}{\partial x_j}\right] + C_{1\varepsilon}\frac{\varepsilon}{k}(G_k + C_{2\varepsilon}G_b) - C_2\rho\frac{\varepsilon^2}{k} + S_\varepsilon \qquad (14)$$

In these equations, G_k represents the generation of turbulence kinetic energy due to the mean velocity gradient. G_b is the generation of turbulence kinetic energy due to buoyancy, Y_M represents the contribution of the fluctuating dilatation in compressible turbulence to the overall dissipation rate, $C_{1\varepsilon}$, $C_{2\varepsilon}$ and $C_{3\varepsilon}$, are constants. σ_k and σ_ε are the turbulent Prandtl numbers for k and $\boldsymbol{\varepsilon}$, respectively. (ANSYS , 2012). Where G_k and G_b are defined in (15) and (16) respectively.

$$G_k = \tau_{ij}\frac{\partial u_i}{\partial x_j} = -\rho\overline{u_i' u_j'}\frac{\partial u_i}{\partial x_j} \qquad (15)$$

$$G_b = \beta g_i \frac{\mu_t}{Pr_t}\left(\frac{\partial \theta}{\partial x_i}\right) = \beta g_i \frac{\mu_t}{Pr_t}\left(\frac{\partial T}{\partial x_i} - \frac{g_i}{c_p}\right) \qquad (16)$$

Where $\frac{g_i}{c_p}$ is the adiabatic lapse rate (ALR), if $\frac{\partial T}{\partial x_i}$ es grater tan the ALR it represents an unstable stratification, else if $\frac{\partial T}{\partial x_i}$ es less than the ALR then turbulence will be suppressed from the atmosphere resulting in a stability condition. (Alinot and Masson, 2005). Some modifications to this model are suggested to achieve an accurate representation of turbulence in the atmosphere as proposed by Pieterse and Harms (2010) with the values for k and ε presented in table 5 depending on the atmospheric condition.

Chapter 3

Methodology

Aiming to study the effects of the atmospheric stability conditions on the pollutant concentration downwind roads, we selected the simplest possible geometry (a road on a horizontal area without any obstacle to the wind flow) and observed the dispersion of the pollutants emitted by vehicles under different atmospheric stability conditions. We solved numerically the physics equation that govern the dispersion of solid and gas phase pollutants using a CFD commercial software (ANSYS Fluent). The atmospheric stability conditions were simulated following the Monin Obukhov Similarity Theory (MOST). This step implies the specification of i.) the wind speed and temperature profiles in the SL, and ii.) the appropriate turbulence model. Next, we describe each of these steps.

Following up the previous work simulating the dispersion of pollutant near roads under neutral atmospheric conditions (Huertas and Prato, 2019), we selected the simplest possible geometry, which is a road located on a flat region without any obstacle to the dispersion of the pollutants. Then, for this geometry we defined the computational domain shown in Fig 3.1, which is a box 5 m deep, 330 m long and 50 high. These dimensions were selected according to Franke et al. (2007) who recommended the minimum dimensions of the computational domain in the way that the walls do not interfere with the dispersion of the pollutants.

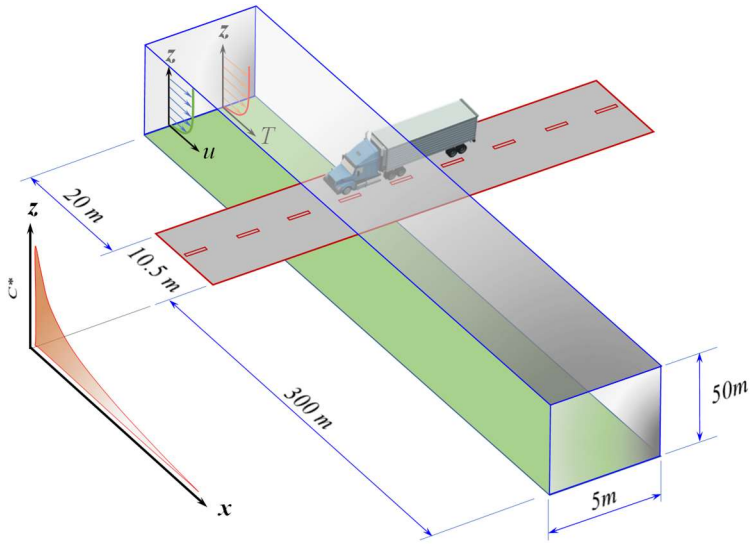

Figure 3. 1 Computational domain used for this study. Length scale is not uniform on the illustration.

Pollutants: the transit of the vehicles over the road generate pollutants that are emitted from the vehicle´s tailpipe and from the interaction road-wheels. Authors separate the process of dispersion of these pollutants in two steps: i.) from the tailpipe (or wheel) to the road, and ii.) from the road to ambient. Our work concentrates in the second step. Since the works conducted modelling the first step (Wang and Zhang, 2009) still do not describe the resulting

on the road, long term average, pollutant concentrations, we assumed they can be represented by an emission distributed uniformly on the road surface. For comparative purposes, we chose an arbitrary emission of E_b = 1 g/s m^2 and verified that results do not depend on the selection of the emission rate.

Chemical reactions were not considered in the model, which is an acceptable assumption for the case of inert pollutants or pollutants with mean lifetime (L_t) much longer that the residence time within the computational domain (R_t). For a wind speed of 1 m/s, the residence time of the pollutants in our computational domain is ~5.5 minutes.

Based on the experimental work of Huertas et al. (ME Huertas, Huertas, & Valencia, 2017) we modelled particles that follows a Rossin Ramler particle size distribution with a maximum diameter of 34 μm, minimum diameter of 1μm, average diameter of 8.5 μm and a dispersion parameter of 3, this parameter describes how the particle diameter range varies to the mean diameter, if n is large then the range of range of particle is very near to mean diameter. We also used the *Discrete Random Walk model (DRW)* to observe particle dispersion. This model is a zeroth-order stochastic tracking method that starts with the velocity flow field obtained by solving the Navier-Stokes equations. Then, the random walk model integrates Equations 1 and 2 to predict particle trajectory, using the local continuous phase conditions as the particle moves through the flow, for a sufficient number of representative particles. (ANYS, 2012)

$$\frac{du_p}{dt} = F_D + \frac{g_z(\rho_p - \rho)}{\rho_p} + F \qquad (17)$$

$$F_D = \frac{18\mu}{\rho_p\, d^2}\,\frac{C_d Re}{24}\left(u - u_p\right) \qquad (18)$$

3.1 Simulation of the atmospheric dynamics

Wind speed: The wind speed inlet profiles for the different atmospheric stability conditions were computed following (4) and are presented in Figure 3.2a

Temperature: As mentioned before the temperature profiles follows a logarithmic profile described in (5) and shown in Figure 3.2b

Some initial conditions have been based on the study conducted by Pieterse and Harms (2013) (Table 3.1) for different atmospheric stability conditions and from this the input profiles for wind speed and temperature were developed, some parameters were modified to fit the conditions of the domain studied in (Huertas and Prato, 2019) and the height of the present computational domain.

Table 3.1 Parameters to describe Atmospheric Stability Conditions

Atmospheric Stability Class	T_o	L	u_*	k	ε	Stability factor f_s	
	K	m	m/s	m/s^2	m^2/s^2	TSP	Gases
Extremely Unstable	313	-108	0.497	5.5069	0.003368	0.77	0.82
Slightly unstable	305	-10000	0.485	3.8536	0.002751	0.64	0.75
Neutral	298	∞	0.53	1.2699	0.000544	1.00	1.00
Slightly Stable	283	310	0.472	1.1089	0.003838	1.07	0.98
Extremely Stable	280	10	0.467	1.0053	0.004277	1.31	1.85

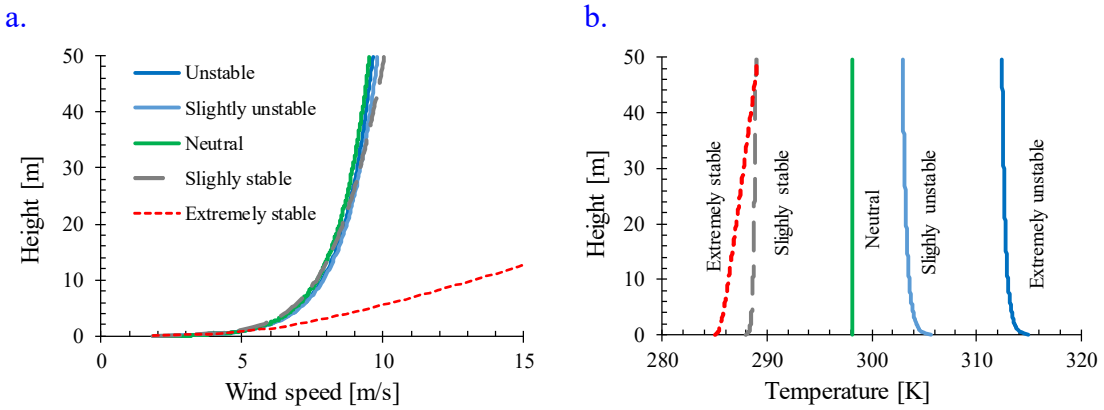

Figure 3. 2 Inlet profiles for extremely unstable, slightly unstable, slightly stable and extremely stable conditions for a) Wind speed b) Temperature

3.2 Dimensional analysis

Wind speed has a strong influence of pollutant dispersion. Wind with low speeds is a typical condition of stable atmospheres, while wind with high speeds is a typical condition of unstable atmospheres.

To isolate the effects of wind speed from the effects of the other variables that influence the conditions of atmospheric stability, we report results in terms of the nondimensional numbers developed by Huertas and Prato (2019). They demonstrated that, for neutral atmospheres, when pollutant concentrations downwind the road are expressed in terms of the nondimensional number for concentration (C^*, (19)) and distance to the road (x^*, (20)), the resulting profiles are independent of wind speed (U) and emission rates (E). Therefore, potential variations on that universal profile are attributed to variations on the atmospheric stability conditions rather than variations on wind speeds.

$$C^* = \frac{C\,U}{E} S_c \qquad (19)$$

$$x^* = \frac{x}{W} \quad (20)$$

Where W is the road width (10.5 m) and $Sc = \upsilon/D$ is the Schmidt which is the ratio of momentum diffusivity (kinematic viscosity, υ) and mass diffusivity (D), and is used to characterize fluid flows in which there are simultaneous momentum and mass diffusion convection processes.

3.3 Statistical analysis

Fox (1984), Hanna (1989), Hanna et al (1991;1993) and ASTM (2000) proposed some comprehensive model performance measures for air quality and dense-gas dispersion models. Measures such as the fractional bias (FB), the normalized mean square error (NMSE), the geometric mean (MG) have been accepted and recommend by the United States Environmental Protection Agency (USEPA) for model evaluation.

Normalized Mean Square Error: The normalization assures that the NMSE will not be biased towards models that over predict or under predict. Smaller values of NMSE denote better model performance.

$$NMSE = \frac{\overline{(C_0 - C_P)^2}}{\overline{C_0} \times \overline{C_P}} \quad (21)$$

Fractional Bias: Boylan and Russell (2006) promoted the use of fractional statistics for PM in part because of their convenient features (bounded by ±2). Where 0 represents a "perfect model".

$$FB = 2 \times \left(\frac{\overline{C_0} - \overline{C_P}}{\overline{C_0} + \overline{C_P}} \right) \quad (22)$$

Geometric Mean Bias: When a data set contains several pairs of data, this logarithmic form of bias is appropriate because underpredictions and overpredictions receive equal weight. A "perfect" model would have MG=1, but MG=1 does not mean that predictions coincide with measurements. An MG greater than 1 implies that the model overestimates and an MG less than 1 that the model underestimates. (Hanna et al., 1993).

$$MG = e^{(\overline{\ln C_0} - \overline{\ln C_P})} \quad (23)$$

Where C_0 is the concentration from the base case and C_P is the predicted concentration from the CFD model for (21) (22) (23)

Chapter 4

Results

As a first step and aiming to ensure that the conservation principle of the Monin Obukhov similarity theory for the horizontal flows of momentum and energy were met, we run our model without any emission from the road for the 5 stability conditions considered in this study. We observed the evolution of wind speed and temperature vertical profiles along the computational domain and confirmed that they remained essentially unaltered, as expected. Figure 4.1 shows those vertical profiles for the case of a neutrally stratified atmosphere. Some negligible deviations from the inlet profiles are observed near the ground surface, which are due mainly to the refinement in the mesh on that region.

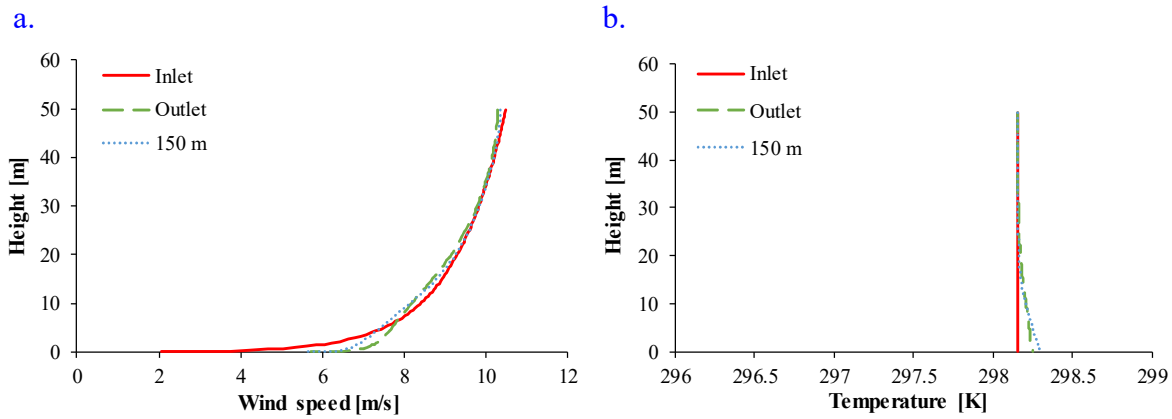

Figure 4. 1 (a)Wind speed, (b) and temperature profile horizontal conservation for neutral stability condition at inlet (solid line), 150 m downwind (dotted line), outlet (dashed line)

Then we added emissions from the road and observed the dispersion of solid and gas phase pollutants emitted from the road under 5 cases of atmospheric stability conditions: extremely unstable, slightly unstable, neutral, slightly stable and extremely stable. We used a base case of comparison the neutral atmospheric condition, where the temperature is uniform along the computational domain.

For the case of neutral atmospheric conditions, figures 4.2a-b show the variations on the vertical profiles of wind speed and turbulent kinetic energy, respectively, at several locations downwind resulting from the mixing of the pollutants emitted from the road and the incoming wind flow. They show that the emissions from the road disturb the atmospheric conditions at the edge of the road and that those perturbations tend to disappear with the distance to the road. Similarly, Figure 4.2c illustrates the concentration profiles resulting from the action of the wind dispersing the pollutants emitted from the road. Figure 4.2d shows the resulting concentration profile at the ground surface and at a critical distance above ground for applications on human health studies (2m). These figures show that the pollutant concentration at the edge of the road reach their maximum values and then reduce toward a stable value far away from the road.

Keeping constant the emission rate and atmospheric conditions, Figure 4.2e shows the variation of those ground pollutant concentrations with wind speed. It shows that the pollutant (in this case TSP) concentration at the road edge reduces from ~20 to ~2 gr/m^3 per unit emission rate (gr/s m^2) when wind speed increases from 0.1 to 5 m/s, which represents a ~1000% variation due to variations in wind speed. Figure 4.2f shows the same results but expressed in terms of C^* and x^*. It shows that the concentration profiles downwind the road fall into a single universal profile when represented in terms of those dimensional numbers for both solid and gas phase pollutants. Furthermore, it demonstrates that C^*, at any distance downwind the road, is independent of wind speed, which means that according to (19) pollutant concentration (C) is inversely proportional to with windspeed. Huertas et al (2019) also demonstrated that C^* is independent of the emission rate and the pollutant under consideration. However, we highlight that these conclusions are valid only for the case of the dispersion of pollutant from roads located on flat terrain and without any obstacle to pollutant dispersion.

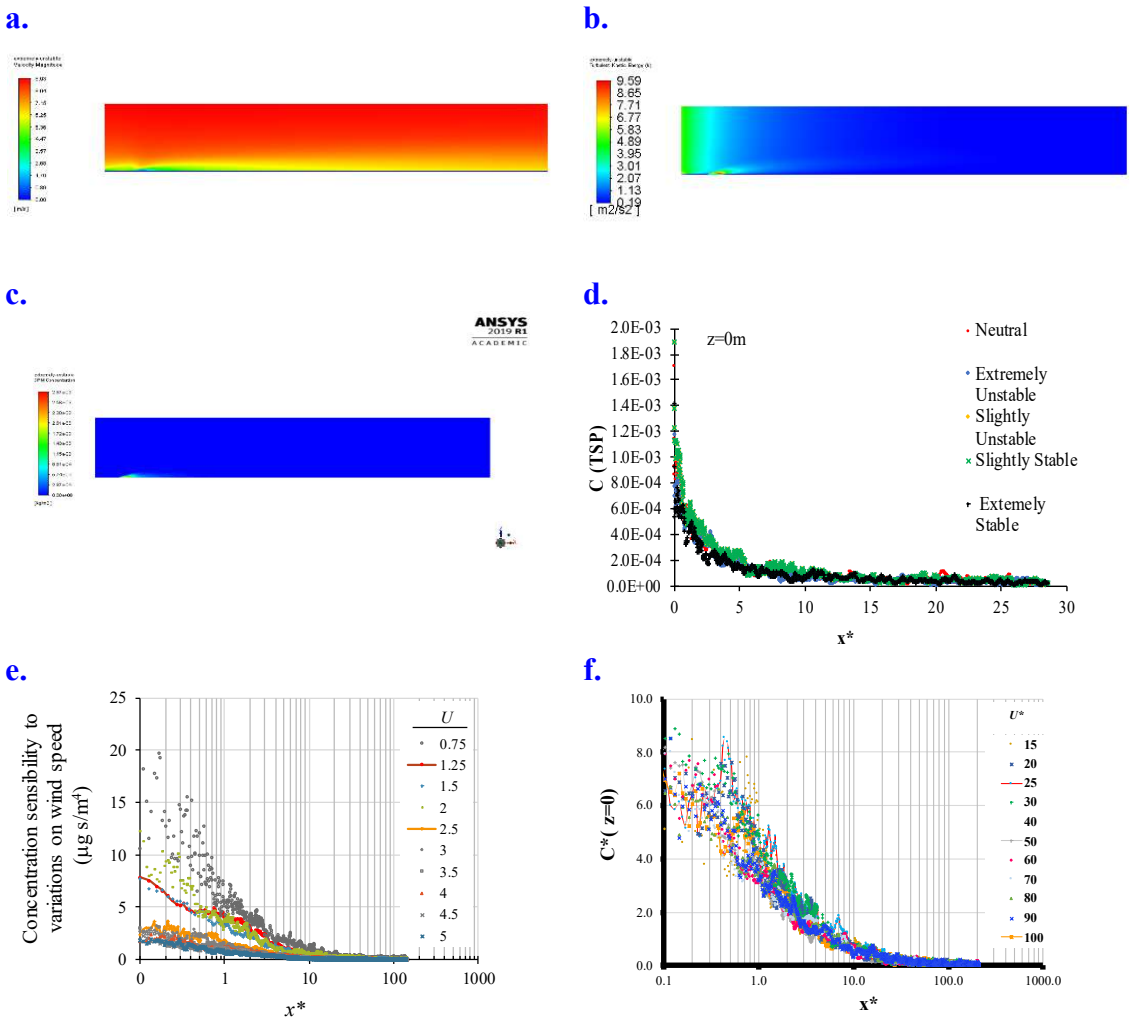

Figure 4. 2 a) velocity contour, b) turbulent kinetic energy contour c) TSP concentration contour for atmospheric condition of extremely unstable, d) Horizontal concentration profile C $[\mu g/m^3]$ vs x and e) Sensibility analysis for wind speed variation f) Horizontal concentration profile C* vs x* e) and f) taken from (Huertas and Prato, 2019)*

Comparison with experimental results

Aiming to validate our CFD based model for the dispersion of pollutants near roads (NR-CFD model) we compared results of this model with the experimental data obtained by the NOAA in 2008 (Clawson et al., 2009) and reported by Finn et al. (2010) and Steffens et al. (2013).

Figure 5.b shows the box plot of the 15 minutes SF_6 concentrations measured at 3, 4, 6, 8, 11,15, 20 and 30 m downwind a 54 m line emission source of 51.0 or 30.5 mg/s of SF_6 under atmospheric neutral conditions and 18 conditions of wind speed in the range of 3.3 – 8.1 m/s (Figure 4.3.a). We adopted an equivalent road width of 1 m and a Smidt number for SF_6 of 0.207 to express these experimental results in terms of C^* and x^*. Figure 4.3.b also includes the NR-CFD model results obtained for the dispersion of a line source of SF6 under similar

conditions (neutral atmospheric conditions, wind speed of 6 m/s, and emission of SF_6 of 51 mg/s). Furthermore, this figure also includes the dispersion of NOx from a 10.5 m width road under neutral atmospheric conditions and 10.4 m/s of average wind speed. We used Sc=0.946 for this NOx. Qualitatively all results fall within the same curve when expressed in terms of C^* and x^*. Figure 4.3.c shows that those results are highly correlated (R^2>0.99) and with similar values (slope~1). These results demonstrate the capacity of the NR-CFD model of reproducing short term steady state experimental measurements.

This study presents a correlation coefficient (R^2> 0.91), Fractional Bias (FB) = 0 in all comparisons, Normalized Mean Square Error (NMSE) 0.02 [g / m^3] for the slightly stable case, 0.1[g / m^3] when the atmosphere is in an extremely stable condition, 0.1[g / m^3] for slightly instability and 0.01 [g / m^3] for the case of extremely instability and Geometric Bias for the stable case and unstable case of 1.00 and 1.02 respectively.

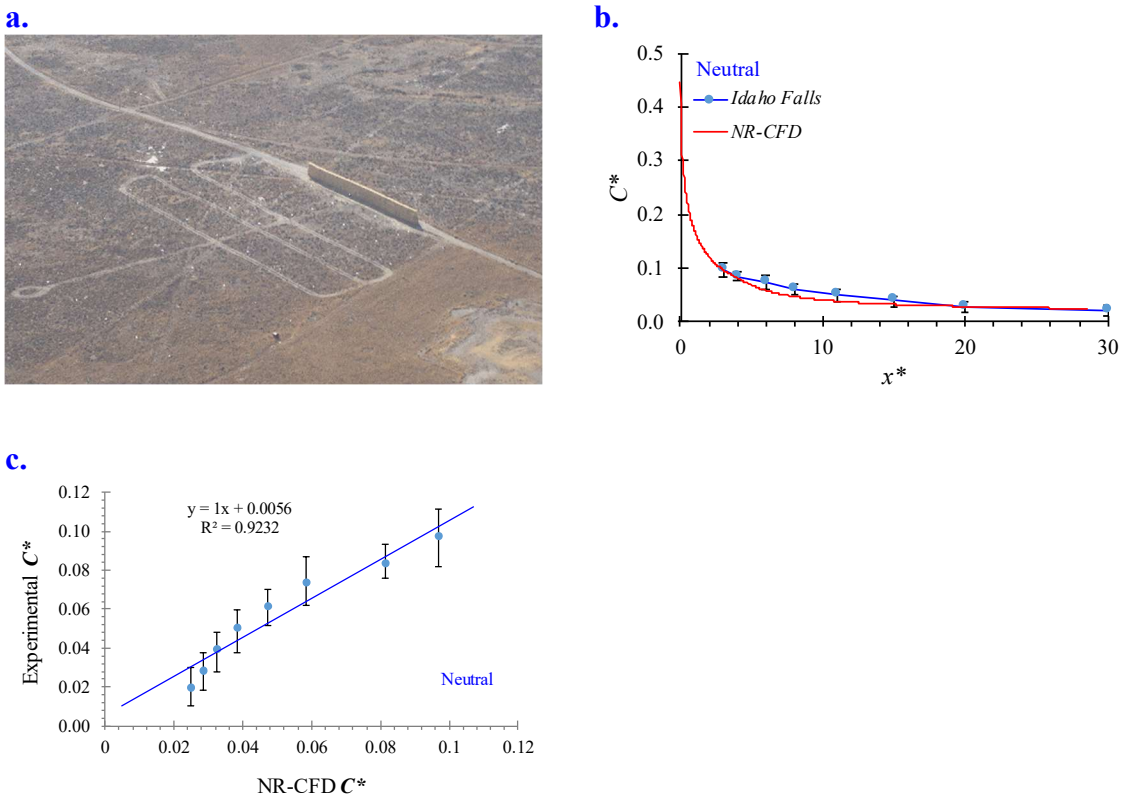

Figure 4. 3 Comparisson of NR-CFD model results with experimental measurements obtained in Idaho Falls experiment conducted by NOAA (2008) a) Ilustration of the experiment taken from Clawson et al (2008) b) C* for NR-CFD and experimental measurements for a Neutral atompheric condition c) Regression analysis between experimental C* and NR-CFD C*

Effects of the atmospheric stability conditions on pollutant dispersion

Finally, we used the NR-CFD model to study systematically the effects of the atmospheric conditions on the dispersion of pollutants near roads. Figures 4.4.a-b show the horizontal concentration profiles at ground level (C^* vs x^*) for solid and gas phase pollutants under different conditions of atmospheric stability. They show small differences in the horizontal concentration profiles due to variations on the atmospheric stability conditions that decrease with distance to the road. Aiming to quantify those differences, for the case of particle dispersion, Figures 4.3.a-c show that horizontal pollutant concentration near road are highly correlated at different atmospheric conditions of stability with the obtained under neutral conditions of stability ($R^2 > 0.91$). Figures 4.3.a-c and Table 3.1 show that extremely unstable atmospheric conditions lead to concentrations ~23% smaller when compared to neutral conditions (slope ~ 0.75), while extremely stable conditions lead to concentrations ~30% higher that the obtained under neutral conditions. When the atmosphere is in a slightly unstable or in a slightly stable condition, TSP concentrations are ~ 35% smaller, and ~ 7% greater, respectively, than when the atmosphere is in a neutral condition. Figure 4.3.a-c also show that those variations remain similar at 2 m above ground. Similar results were also obtained for the case of gas phase pollutants (Table 3.1).

These variations are much smaller than the ones resulting from variations of wind speed, which according to Figure 4.4 range from 200%-2000% at the edge of the road and becomes negligible (< 1%) far away from the road (>100 x^*). Figure 4.4 was obtained as $dC^*/dU = C\ Sc/E$ from the results simulating particle dispersion for several wind speeds for the case of neutral atmospheric conditions.

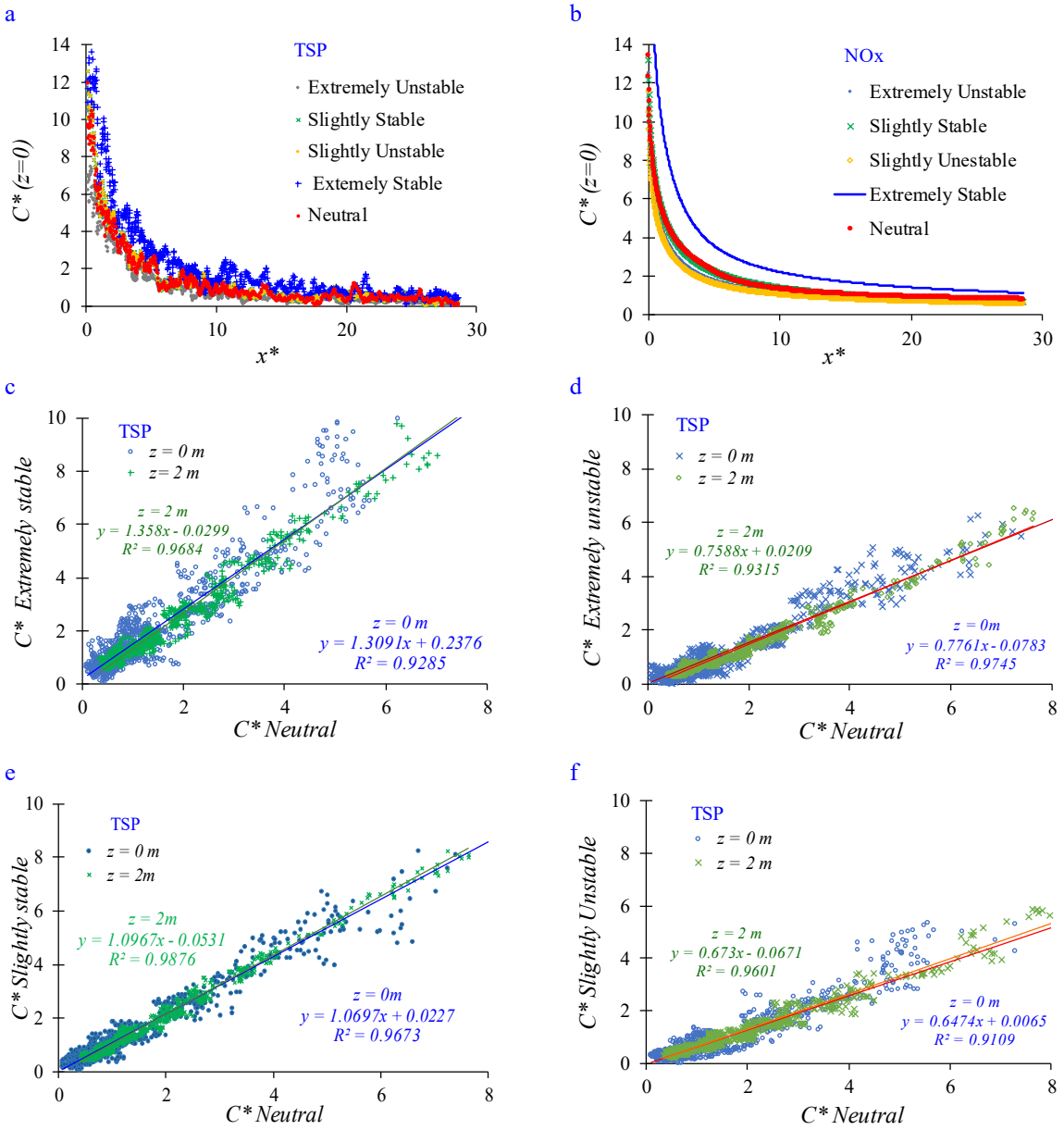

Figure 4. 4 *Horizonal dimensionless concentration profiles for a) TSP at surface level (z=0); b) gas phase pollutants at z=0 under different the atmospheric conditions. Correlation between the dimensionless downwind TSP concertation at surface level and at z=2 m obtained under neutral atmospheric conditions and c) extremely stable, d) extremely unstable, e) slightly stable, and f) slightly unstable atmospheric conditions.*

Chapter 5

Conclusion

Current near road pollutant dispersion models have been criticized because they neglect the influence of the different atmospheric stability conditions. It has been counter-argued that at the local microscale level, near ground, the flow field is mainly influenced by the mechanical turbulence generated by the presence of physical obstacles like the surface roughness or buildings which disturb the free wind flow, while atmospheric stability conditions result from the heat transfer interactions between the ground surface and the air flow under the presence or absence of sunlight, and therefore it is a meso-scale or regional phenomena with minor effect on the near road pollutant dispersion. The discussion becomes even more complex when it is taken into consideration that low wind speeds are associated to stable atmospheres while high wind speeds are associated to unstable atmospheres.

Solving numerically, via CFD, the governing equations that describe the dispersion of pollutants emitted by the transit of vehicles, we evaluated systematically the influence of the atmospheric stability conditions on the nearby resulting pollutant concentration. The atmospheric stability conditions were simulated: i.) following the Monin Obukhov Similarity Theory which specifies the vertical profiles for wind speed and temperature, and ii.) using the k-ε standard turbulence model calibrated experimentally for each atmospheric stability conditions by Pieterse and Harms. To isolate the effects of wind speed on pollutant dispersion we reported results in terms of dimensionless number of concentration (C*,(19)) and distance to the road (x*, (20)) obtained by Huertas and Prato (2019). They demonstrated that, for neutral atmospheres, when pollutant concentrations downwind the road are expressed as C^* *vs* x^* the resulting profiles are independent of wind speed and emission rates. Therefore, potential variations on that universal profile are attributed to variations on the atmospheric stability conditions rather than variations on wind speeds.

For the case of particles, we observed that the C^* obtained under different atmospheric stability conditions are highly correlated (R^2 >0.91) to the C^* obtained under neutral conditions. We also observed that when the atmosphere is extremely stable or slightly stable, C^* increase 30% and 7%, respectively. Contrarily, when the atmosphere is extremely unstable or slightly unstable, C^* decrease 35% and 23%, respectively. Similar results were obtained for the case of gas phase pollutants. These variations are much smaller than the ones resulting from variations of wind speed, which range from 200%-2000% at the edge of the road and becomes negligible (< 1%) far away from the road (<100 x^*). These results agree with experimental results obtained by Finn et al observing the dispersion of HS_6 near roads under different atmospheric stability conditions.

We propose to affect C^* by a factor (f_s, Table 3.1) to include the effects of the atmospheric stability conditions on pollutant dispersion near road, where C* continue being the dimensionless number for pollutant concentration near roads obtained under neutral atmospheric conditions.

Appendix A

Abbreviations and acronyms

	Description
ABL	Atmospheric boundary layer
ALR	Adiabatic Lapse Rate
CFD	Computational fluid dynamics
FB	Fractional Bias
GB	Geometric Bias
LES	Large Eddy Simulation
MOST	Monin-Obukhov Similarity Theory
NMSE	Normalized Mean Square Error
PM	Particulate matter
PM_{10}	Particulate matter with aerodynamic diameter < 10 mm
$PM_{2.5}$	Particulate matter with aerodynamic diameter < 2.5 mm
RANS	Reynolds Averaged Navier Stokes
RMSE	Root Mean Square Error
SL	Surface layer
TSP	Total Suspended Particles (Particulate matter with aerodynamic diameter <30 mm)

Appendix B

Variables and Symbols

Variable	*Description*	*Units*
C	TSP concentration at surface level	$\mu g/m^3$
C^*	Dimensionless TSP concentration	-
C_0	Pollutants concentration in base case	$\mu g/m^3$
C_p	Predicted Pollutants concentration	$\mu g/m^3$
c_p	Air Specific Heat Capacity at constant pressure	$J/K\ kg$
E	TSP mass emission rate per road area	$g\ /s\ m^2$
ε	Turbulence Dissipation rate	m^2/s^2
F_d	Dispersion factor	-
g_z	Gravity	m/s^2
H_0	Heat flux from the surface	W/m^2
K	Von Karman universal constant	-
κ	Turbulence Kinetic Energy	m/s^2
L	Obukhov's Length	m
L_t	Pollutant life time	s
μ	Fluid molecular viscosity	$kg/m{\cdot}s$
$\rho,\ \rho_p$	Fluid and particle density	kg/m^3
R_t	Pollutatn Residence time	s
T_o	Temperature at surface	K
u	Wind speed at height z	m/s
u^*	Friction velocity	m/s
U	Mean wind speed in the x direction	m/s
U^*	Dimensionless speed ratio	-
W	Road width	m
w_{po}	Particle emission speed	m/s
x	Distance from the road edge	m
x^*	Non dimensional distance to the road edge	-
z	Height	m
z_o	Surface roughness	m
Γ	Adiabatic Lapse Rate	K/m
Λ	Environmental Lapse rate	K/m
ψ_m	Similarity Function	-
ψ_h	Similarity Function	-
ζ	Buoyancy parameter (z/L)	-

Bibliography

Alinot, C., & Masson, C. (2005). k-ε Model for the Atmospheric Boundary Layer Under Various Thermal Stratifications. *Journal of Solar Energy Engineering*, *127*(4), 438. https://doi.org/10.1115/1.2035704

ANSYS FLUENT. (2012). Theory guide. ANSYS, Inc.

Arya, S. (1988). Introduction to micrometeorology. Academic Press

Ashrafi, K., & Hoshyaripour, G. a. (2008). A Model to Determine Atmospheric Stability and its Correlation with CO Concentration. *International Journal of Environmental and Ecological Engineering*, *2*(8), 96–101. https://doi.org/scholar.waset.org/1999.6/9007

ASTM (2000) Standard guide for statistical evaluation of atmospheric dispersion model performance. American Society for Testing and Materials, Designation D 6589- 00. ASTM, 100 Barr Harbor Drive, West Conshohocken, PA 19428-2959

Baldauf, R. W., Isakov, V., Deshmukh, P., Venkatram, A., Yang, B., & Zhang, K. M. (2016). Influence of solid noise barriers on near-road and on-road air quality. *Atmospheric Environment*, *129*, 265–276. https://doi.org/10.1016/j.atmosenv.2016.01.025

Barratt, R. (2001). Atmospheric dispersion modelling: An introduction to practical applications. London: Earthscan.

Businger, J.A., Wyngaard, J., Izumi, Y., Bradley, E., 1971. Flux-profile relationships in the atmospheric surface layer. *Journal of the Atmospheric Science* 28,181-189.

Clawson, K.L., Eckman, R.M., Johnson, R.C., Carter, R.G., Finn, D., Rich, J.D., Hukari, N. F., Strong, T., Beard, S.A., Reese, B.R., 2009. Near Roadway Tracer Study (2008). NOAA Technical Memorandum OAR ARL-260, Air Resources Laboratory, Idaho Falls, Idaho.

Dyer, A. J. (1974). A review of flux-profile relationships. *Boundary-Layer Meteorology*, *7*(3), 363–372. https://doi.org/10.1007/BF00240838

De Visscher, Alex. (2013). *Air Dispersion Modeling. Foundations and Applications.* 10.1002/9781118723098.ch6.

Eckman, R. M., Rich, J. D., Perry, S. G., Carter, R. G., Clawson, K. L., Isakov, V., … Heist, D. K. (2009). Tracer studies to characterize the effects of roadside noise barriers on near-road pollutant dispersion under varying atmospheric stability conditions☆. *Atmospheric Environment*, *44*(2), 204–214. https://doi.org/10.1016/j.atmosenv.2009.10.012

Franke, J., Hellsten, A., Schlnzen, H., Carissimo, B. (2007) Best practice guideline for the CFD simulation of flows in the urban environment. In: COST Action 732: Quality Assurance and Improvement of Microscale Meteorological Models, COST Office, Brussels, ISBN:3-00-018312-4.

Fox DG (1984) Uncertainty in air quality modeling. B Amer Meteor Soc 65: 27–36

Hagler, G. S. W., Lin, M. Y., Khlystov, A., Baldauf, R. W., Isakov, V., Faircloth, J., & Jackson, L. E. (2012). Field investigation of roadside vegetative and structural barrier impact on near-road ultrafine particle concentrations under a variety of wind conditions. *Science of the Total Environment*, *419*, 7–15. https://doi.org/10.1016/j.scitotenv.2011.12.002

Hanna SR (1989) Confidence limits for air quality model evaluations as estimated by bootstrap and jackknife resampling methods. Atmos Environ 23: 1385–1398

Hanna SR, Chang JC, Strimaitis DG (1993) Hazardous gas model evaluation with field observations. Atmos Environ 27A: 2265–2285

Hanna SR, Strimaitis DG, Chang JC (1991) Hazard response modeling uncertainty (A quantitative method), vol. I: User's guide for software for evaluating hazardous gas dispersion models; vol. II: Evaluation of commonly used hazardous gas dispersion models; vol. III: Components of uncertainty in hazardous gas dispersion models. Report no. A119=A120, prepared by Earth Tech, Inc., 196 Baker Avenue, Concord, MA 01742, for Engineering and Services Laboratory, Air Force Engineering and Services Center, Tyndall Air Force Base, FL 32403; and for American Petroleum Institute, 1220 L Street, N.W., Washington, D.C., 20005

Huertas J.I., Huertas M.E., Solis, C. (2012) Characterization of airborne particles in an open pit mining region. *Science of the total Environment*. 423:39–46.

Huertas Cardozo, J. I., & Prato Sánchez, D. F. (2019). An experimental and numerical study of air pollution near unpaved roads. *Air Quality, Atmosphere & Health*. https://doi.org/10.1007/s11869-019-00678-9

Huertas, M.E., Huertas, J.I., Valencia, A. (2017) Vehicular road influence areas. *Atmospheric Environment*, 151:108–116.

Jeong, S. J., & Ra Kim, A. (2018). CFD study on the influence of atmospheric stability on near-field pollutant dispersion from rooftop emissions. *Asian Journal of Atmospheric Environment*, *12*(1), 47–58. https://doi.org/10.5572/ajae.2018.12.1.047

Karner, A. A., Eisinger, D. S., & Niemeier, D. A. (2010). Near-roadway air quality: Synthesizing the findings from real-world data. *Environmental Science and Technology*, *44*(14), 5334–5344. https://doi.org/10.1021/es100008x

McConnell, R., Berhane, K., Yao, L., Jerrett, M., Lurmann, F., Gilliland, F., … Peters, J. (2006). Traffic, susceptibility, and childhood asthma. *Environmental Health Perspectives*, *114*(5), 766–772. https://doi.org/10.1289/ehp.8594

Mohan, M., & Siddiqui, T. A. (1998). Analysis of various schemes for the estimation of atmospheric stability classification. *Atmospheric Environment*, *32*(21), 3775–3781. https://doi.org/10.1016/S1352-2310(98)00109-5

Niita, H. I. R., Sato, T., Nakai, S., Maeda, K., Aokl, S. H., & Ono, M. A. (1993). Respiratory health associated with exposure to automobile exhaust. 1. results of cross-sectional studies in 1979, 1982, and 1983. *Archives of Environmental Health*, *48*(1), 53–58. https://doi.org/10.1080/00039896.1993.9938393

Obukhov, A. M. (1971). Turbulence in an atmosphere with a non-uniform temperature. *Boundary-Layer Meteorology*, *2*(1), 7–29. https://doi.org/10.1007/BF00718085

Oke, T.R. (1987) Boundary Layer Climates. 2nd Edition, Methuen Co., London, New York, 435.

Pasquill, F. (1961) The Estimation of the Dispersion of Windborne Material. *Meteorological Magazin,* 90, 33-49.

Pearson, R. L., Wachtel, H., & Ebi, K. L. (2000). Distance-weighted traffic density in proximity to a home is a risk factor for leukemia and other childhood cancers. *Journal of the Air and Waste Management Association*, *50*(2), 175–180. https://doi.org/10.1080/10473289.2000.10463998

Pieterse, J. E., & Harms, T. M. (2013). CFD investigation of the atmospheric boundary layer under different thermal stability conditions. *Journal of Wind Engineering and Industrial Aerodynamics*, *121*(March), 82–97. https://doi.org/10.1016/j.jweia.2013.07.014

Ranasinghe, D. R., Zhu, Y., Paulson, S., Lee, E. S., Mara, S., Ahangar, F. E., … Amini, S. (2017). Field evaluation of vegetation and noise barriers for mitigation of near-freeway air pollution under variable wind conditions. *Atmospheric Environment*, *175*(November 2017), 92–99. https://doi.org/10.1016/j.atmosenv.2017.11.060

Riediker, M., Cascio, W. E., Griggs, T. R., Herbst, M. C., Bromberg, P. A., Neas, L., … Devlin, R. B. (2004). Particulate matter exposure in cars is associated with cardiovascular effects in healthy young men. *American Journal of Respiratory and Critical Care Medicine*, *169*(8), 934–940. https://doi.org/10.1164/rccm.200310-1463

Seinfeld, J. H., & Pandis, S. N. (2006). *ATMOSPHERIC From Air Pollution to Climate Change SECOND EDITION*. *Atmospheric Chemistry and Physics*.

Singh, S., A. Presto, A., & J. Adams, P. (2018). Simulations of vehicle-induced mixing and near-road aerosol microphysics using computational fluid dynamics. *AIMS Environmental Science*, *5*(5), 315–339. https://doi.org/10.3934/environsci.2018.5.315

Steffens, J. T., Heist, D. K., Perry, S. G., & Zhang, K. M. (2013). Modeling the effects of a solid barrier on pollutant dispersion under various atmospheric stability conditions. *Atmospheric Environment*, *69*, 76–85. Retrieved from http://ovidsp.ovid.com/ovidweb.cgi?T=JS&PAGE=reference&D=emed11&NEWS=N&AN=2013021376

Stull, R. (2010). *Practical Meteorology: An Algebra-based Survey of Atmospheric Science*.

Stull, R. (2005). The Atmospheric Boundary Layer. *An Introduction to Boundary Layer Meteorology*, 375–418.

Tong, Z., Baldauf, R. W., Isakov, V., Deshmukh, P., & Max Zhang, K. (2016). Roadside vegetation barrier designs to mitigate near-road air pollution impacts. *Science of the Total Environment*, *541*, 920–927. https://doi.org/10.1016/j.scitotenv.2015.09.067

Toparlar, Y., Blocken, B., Maiheu, B., & van Heijst, G. J. F. (2017). A review on the CFD analysis of urban microclimate. Renewable and Sustainable Energy Reviews, 80(September 2016), 1613–1640. https://doi.org/10.1016/j.rser.2017.05.248

Turner, D. (1979). Workbook of Atmospheric Dispersion Estimates, AP-26. *US EPA, Office of Air Programs. Research Triangle*. Retrieved from

http://scholar.google.com/scholar?hl=en&btnG=Search&q=intitle:Workbook+of+atmospheric+dispersion+estimates#1

Wang, F., Chambers, S. D., Zhang, Z., Williams, A. G., Deng, X., Zhang, H., … Allegrini, I. (2016). Quantifying stability influences on air pollution in Lanzhou, China, using a radon-based "stability monitor": Seasonality and extreme events. *Atmospheric Environment*, *145*, 376–391. https://doi.org/10.1016/j.atmosenv.2016.09.014

Wang, Y. J., & Zhang, K. M. (2009). Modeling near-road air quality using a computational fluid dynamics model, CFD-VIT-RIT. *Environmental Science and Technology*, *43*(20), 7778–7783. https://doi.org/10.1021/es9014844

Zoras, S., Triantafyllou, A. G., & Deligiorgi, D. (2006). Atmospheric stability and PM10 concentrations at far distance from elevated point sources in complex terrain: Worst-case episode study. *Journal of Environmental Management*, *80*(4), 295–302. https://doi.org/10.1016/j.jenvman.2005.09.010